Hexagonal Tungsten Oxide Based Electrochromic Devices: Spectroscopic Evidence for the Li Ion Occupancy of Four-Coordinated Square Windows

Subramanian Balaji,[†] Yahia Djaoued,*[,†] André-Sébastien Albert,[†] Richard Z. Ferguson,[†] and Ralf Brüning[‡]

Laboratoire de Micro-spectroscopies Raman et FTIR, Université de Moncton—Campus de Shippagan, 218, boul. J.-D. Gauthier, Shippagan, New Brunswick, E8S 1P6, Canada, and Physics Department, Mount Allison University, Sackville, New Brunswick, E4L 1E4, Canada

Received December 21, 2008. Revised Manuscript Received February 19, 2009

Macroporous hexagonal WO_3 (h-WO_3) films were obtained at 400 °C from a sol containing tungstic acid with organically modified silane as a template. Asymmetric electrochromic devices based on the macroporous h-WO_3 layer were constructed. XRD and micro-Raman studies of the intercalation/deintercalation of lithium into the h-WO_3 layer of the device as a function of the applied voltages were performed. In h-WO_3, Li^+ can be intercalated into three potential sites: trigonal cavity (TC), hexagonal window (HW), and four-coordinated square window (SW). XRD measurements show systematic changes in the lattice parameter, which was associated with the amount of Li intercalated into the h-WO_3 layer. Correspondingly, Raman spectroscopy shows that at 1.0 V Li^+ completely fill TC and partially fill HW sites. For potentials $\geq$1.5 V, Li^+ are inserted into the SW, as evidenced from the vanishing of the ν(O−W−O) Raman modes. The reversible characteristics of the device from optical measurements and Raman spectra demonstrated that the coloration process in the electrochromic device is mainly due to the Li^+ that occupy HW and SW sites of the h-WO_3. Optical measurements performed as a function of applied potentials, show excellent contrasts between colored and bleached states and qualifies the macroporous h-WO_3-based device for smart window applications.

Introduction

Electrochromic (EC) windows are devices that are able to change their optical properties (coloring/bleaching) in a reversible and persistent manner under the action of a small voltage.[1,2] Tungsten oxide (WO_3), due to its multiple oxidation states, is the most widely studied EC material. The optical changes in the EC windows constructed using this material are due to the ion/electron intercalation (double injection) in which various degrees of reversible coloration can be induced along with the possibility of wavelength selectivity. Such windows are capable of regulating the inflow of radiant energy in buildings so that an optimum indoor climate is maintained at a minimum demand on paid energy.[3−5]

An EC device configuration is generally four- or five-layered. At its heart is the WO_3 layer, where the reversible optical change occurs. An asymmetric EC device consists of an ion-conducting (IC) layer, which also acts as the counterelectrode, and a WO_3 EC layer as the working cathode, sandwiched between two transparent conductive electrodes (TE). When a small voltage (1−3 V) is applied across the TE, lithium ions (Li^+) from the counterelectrode and electrons (e^-) from the TE move to the EC WO_3 layer. This double injection of charge carriers results in the formation of Li_xWO_3 bronze, leading to a colored state, and when the polarity of the applied voltages is reversed, Li^+ are deintercalated, leading to a bleached state.[6] The EC phenomenon, occurring with such a double injection of x number of e^- and Li^+, inserted in or ejected out of the system, can be represented as follows:

$$\underset{\text{clear}}{WO_3} + xLi^+ + xe^- \leftrightarrow \underset{\text{dark blue}}{Li_xWO_3}$$

The performance of EC windows depends strongly on the microstructure, crystallinity, crystallite sizes, porosity, thickness, and EC reversibility of the WO_3 layer, as well as its capability for accommodating the guest ions (Li^+).[3] Although amorphous and monoclinic WO_3 (m-WO_3) are the most common phases synthesized and studied as working EC cathodes in EC devices, the hexagonal form of WO_3 (h-WO_3) has received considerable interest as Li ion host material.[7−16]

* Corresponding author. Phone: 1-506-336-3412; Fax: 1-506-336-3477; E-mail: djaoued @umcs.ca.
[†] Université de Moncton—Campus de Shippagan.
[‡] Mount Allison University.

(1) (a) Rosseinsky, D. R.; Mortimer, R. J. *Adv. Mater.* **2001**, *13*, 783–793. (b) http://www.gentex.com.
(2) Granqvist, C. G. *Nature Mater.* **2006**, *5*, 89.
(3) (a) Granqvist, C. G. *Handbook of Inorganic Electrochromic Materials*; Elsevier: New York, 1995. (b) Granqvist, C. G.; Avendano, E.; Azens, A. *Thin Solid Films* **2003**, *442*, 201–211.
(4) Deb, S. K. *Sol. Energy Mater. Sol. Cells* **2008**, *92*, 245–258.
(5) Niklasson, G. A.; Granqvist, C. G. *J. Mater. Chem.* **2007**, *17*, 127–156.
(6) Balaji, S.; Albert, A.-S.; Djaoued, Y.; Brüning, R. *J. Raman Spectrosc.* **2009**, *40*, 92–100.
(7) Cheng, H.; Jacobson, A. J.; Whittingham, M. S. *Solid State Ionics* **1981**, *5*, 355–358.
(8) Cruz, A. M.; Torres-Martinez, L. M.; Garcia-Alvarado, G.; Moran, E.; Alario-Franco, M. A. *Solid State Ionics* **1996**, *84*, 181–188.

10.1021/cm8034455 CCC: $40.75 © 2009 American Chemical Society
Published on Web 03/18/2009

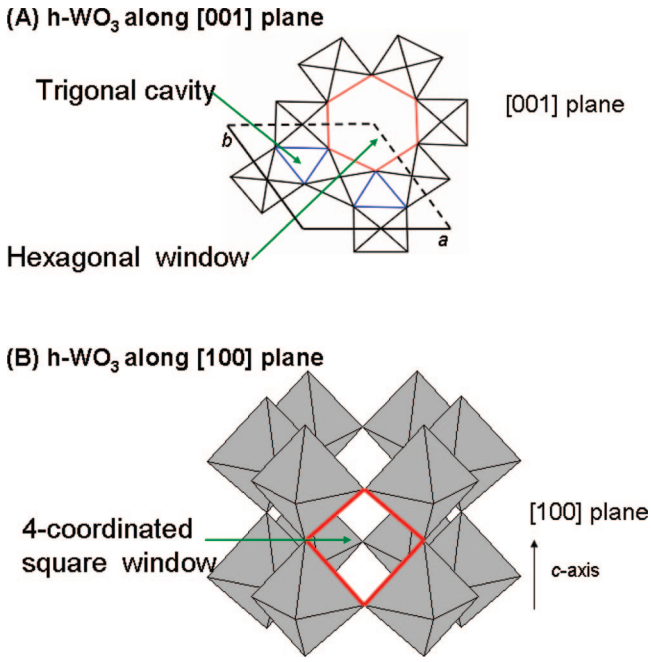

Figure 1. (A) The structure of h-WO_3 is shown with *c* axis perpendicular to the plane. (B) The structure of h-WO_3 with *c* axis parallel to the plane. The figure also shows various Li intercalation sites possible in h-WO_3 (hexagonal and square window, trigonal cavity).

However, the application of h-WO_3 as the active EC layer of an EC device as well as the detailed EC characterization of the device has not been reported. The structure of h-WO_3 is shown in Figure 1. It is constituted by WO_6 octahedra. These octahedra form three- and six-membered rings by sharing the equatorial oxygen in the *ab* plane of WO_6. These structures stack by sharing the axial oxygen in the *c* axis, which results in hexagonal tunnels due to six-membered rings and trigonal tunnels due to three-membered rings. Li ions can be intercalated into the empty hexagonal and trigonal tunnels of h-WO_3 so as to form Li_xWO_3 where *x* can be as large as 3.4, which made this phase interesting for applications in Li ion batteries, gas sensors, EC devices, etc.[10]

Hexagonal WO_3 has been synthesized in a variety of forms, such as powders, nanorods, and thin films by both chemical and physical methods. Synthesis of powder h-WO_3 by reaction between sodium tungstate and hydrochloric acid was first reported by Gerand et al.[17] As an alternative approach, many studies have synthesized h-WO_3 from ammonium (NH_4) based precursors. For example, Han et al. have prepared powder h-WO_3 from $(NH_4)_{10}[H_2W_{12}O_{42}]\cdot 10H_2O$ and provided an overview concerning the preparation of h-WO_3 by NH_4-based precursors.[18] Hexagonal WO_3 prepared by the procedures involving NH_4 has smaller lattice parameter ($c = 0.765$ nm) than the value reported by Gerand et al.[17] ($c = 0.7798$ nm). A hydrothermal procedure has been used by Song et al.[13] to prepare h-WO_3 films at 400 °C. Thermal evaporation was used by Al Mohammad et al.[19] to prepare amorphous WO_3 films that transformed to h-WO_3 upon annealing at 250 °C.

Preparation of porous WO_3 has attracted considerable attention in recent years because of the potential enhancement of the charge transport during double injection. A versatile approach to synthesize porous WO_3 films is based on templating methods that use structure-directing agents. Santato et al. have reported the synthesis of mesostructured WO_3 using PEG 300 as a structure-directing agent.[20] In one of our earlier works, we have reported the preparation of macroporous WO_3 thin films by using polyethylene glycol (PEG) of molar weight 600 as a templating agent.[21a] Recently we have reported the application of pluronic 123 (P-123) for the low-temperature preparation of mesoporous monoclinic WO_3 films and demonstrated their EC switching functionality between bleached and colored states.[21b]

Detailed studies on electrochemical Li insertion into h-WO_3, reported by many researchers, discuss three main aspects: (i) the maximum amount of Li that can be accommodated in h-Li_xWO_3, (ii) the structural changes occurring in the hexagonal framework as a function of Li ion intercalation, and (iii) the analysis of the occupation of the Li ion intercalation sites. While the first two aspects have been investigated by XRD and electrochemical studies, the third one has only been considered theoretically. Unlike larger cations such as K, Cs, Rb, which can occupy only the hexagonal cavity, Li occupies both the trigonal and hexagonal cavities in h-WO_3.[22] According to Slade et al.[23] and Han et al.,[24] three possible locations for intercalated Li, shown in Figure 1A,B, are the trigonal cavity (TC), hexagonal window (HW), and the four-coordinated square window (SW). On the basis of electrochemical and XRD data, there were attempts to determine the possible Li-occupied sites. Hibino et al.[25] calculated electronic energy levels for h-Li_xWO_3 by using the DV-X α method and suggested that the trigonal cavity is the most favorable Li ion insertion site up to $x = 0.4$, as the site energy of the trigonal cavity is slightly less than the energy of the hexagonal window and square window. Although these suggestions are consistent, experimental evidence for the structure of h-Li_xWO_3 with the details of Li ion inserted sites in an electrochemically reversible system is unavailable.

(9) Schlasche, B.; Schollhorn, R. *Rev. Chim. Min.* **1982**, *19*, 534.
(10) Figlarz, M. *Prog. Solid State Chem.* **1989**, *19*, 1–46.
(11) Oi, J.; Kishimoto, A.; Kudo, T. *J. Solid State Chem.* **1992**, *96*, 13–19.
(12) Han, W.; Hibino, M.; Kudo, T. *Bull. Chem. Soc. Jpn.* **1998**, *71*, 933–937.
(13) Song, S.-W.; Kang, I.-S. *Sens. Actuators* **2008**, *129*, 971–976.
(14) Kumagai, N.; Kumagai, N.; Umetzu, Y.; Tanno, K.; Pereira-Ramos, J. P. *Solid State Ionics* **1996**, *86−88*, 1443–1449.
(15) Gu, Z.; Li, H.; Zhai, T.; Yang, W.; Xia, Y.; Ma, Y.; Yao, J. *J. Solid State Chem.* **2007**, *180*, 98–105.
(16) Balázsi, C.; Sedlácková, K.; Llobet, E.; Ionescu, R. *Sens. Actuators* **2008**, *B 133* (2008), 151–155.
(17) Gerand, B.; Nowogrocki, G.; Guenot, J.; Figlarz, M. *J. Solid State Chem.* **1979**, *29*, 429–434.
(18) Han, W.; Hibino, M.; Kudo, T. *Denki Kagaku (J. Electrochem. Soc. Jpn.)* **1998**, *66*, 1230–1233.
(19) Al Mohammad, A.; Gillet, M. *Thin Solid Films* **2002**, *408*, 302–309.
(20) Santato, C.; Odziemkowski, M.; Ulmann, M.; Augustynski, J. *J. Am. Chem. Soc.* **2001**, *123*, 10639–10649.
(21) (a) Djaoued, Y.; Ashrit, P. V.; Badilsecu, S.; Bruning, R. *J. Sol-Gel Sci. Technol.* **2003**, *28*, 235–244. (b) Djaoued, Y.; Priya, S.; Balaji, S. *J. Non-Cryst. Solids* **2008**, *354*, 673–679.
(22) Lee, K.-S.; Seo, D.-K.; Whangbo, M.-H. *J. Am. Chem. Soc.* **1997**, *119*, 4043–4049.
(23) Slade, R. C. T.; West, B. C.; Hall, G. P. *Solid State Ionics* **1989**, *32/33*, 154–161.
(24) Han, W.; Hibino, M.; Kudo, T. *Solid State Ionics* **2000**, *128*, 25–32.
(25) Hibino, M.; Han, W.; Kudo, T. *Solid State Ionics* **2000**, *135*, 61–69.

Although electrochemical and XRD studies have been extensively used for the quantification of the inserted lithium into the h-WO_3, questions regarding lithium intercalation sites in h-WO_3 remain unanswered. However, these studies were not performed in the context of an EC device.

Raman spectroscopy is sensitive to the amorphous, hydrated, and the various allotropic forms (hexagonal, monoclinic, and tetragonal) of WO_3. Intercalation of Li ions into monoclinic WO_3 increases its symmetry. Balaji et al.,[6] Kuzmin et al.,[26] Pyper et al.,[27] and Cazanelli et al.[28] have reported the phase transitions from m-Li_xWO_3 to tetragonal and eventually to the highest-symmetry cubic phase as the amount of intercalated lithium rises. Surprisingly, this sensitive technique has not been utilized for the detailed study of intercalation of lithium into h-WO_3.

In the context of the above presented discussion, in this work, we report (i) a new method to prepare porous h-WO_3 films on an ITO substrate from tungstic acid in the presence of *or*ganically *mo*dified *sil*ane (ORMOSIL) as a templating agent with the objective to use the h-WO_3 films as active electrochromic layers in an operating EC device; (ii) for the first time, a detailed micro-Raman spectroscopic structural characterization of Li ions intercalation/deintercalation into the h-WO_3 layer of an operating EC device as a function of applied coloration/bleaching voltages; and (iii) an XRD characterization of the structural changes occurring during the intercalation/deintercalation of Li ions into the h-WO_3 layer of an operating EC device as a function of applied voltages. Both the Raman and the XRD studies have been performed in conjunction with optical transmittance studies.

Experimental Section

All chemicals in the present work were used as purchased from Aldrich.

Preparation of Sols and Films. Porous films with sufficient thickness were obtained by using hybrid ORMOSIL as a template precursor. ORMOSIL was prepared by reacting *O*,*O*′-bis(2-aminopropyl ether)poly(propyleneglycol) (PPG4000) with (3-isocyanatopropyl)triethoxysilane (ICS) in tetrahydrofuran (THF) in the volume ratio 1:0.1:1. This solution was refluxed for 6 h at 65 °C. After this step, THF was evaporated and pure hybrid ORMOSIL [$(OEt)_3Si$-PPG-$Si(OEt)_3$] was obtained.

WO_3 sols were prepared by reacting 40 mL of H_2O_2 (33%) with 7.5 g of tungsten powder (99.9%). The mixture was left to stir at room temperature for 8 h. After the addition of a small amount of ethanol (EtOH), the sol was refluxed for 4 h at a temperature of 80 °C. Finally, 1.5 g of the hybrid ORMOSIL dissolved in 15 mL of EtOH was added dropwise into the WO_3 sol and the mixture stirred for 1 h. The final sol was used for the WO_3 film coating. WO_3 films were deposited by dip-coating on SiO_2 and ITO-coated-glass substrates at a controlled speed of 4 mm/s. After drying at 60 °C for 2 min, the films were annealed a 400 °C. The samples were held at the peak temperature for 1 h and then cooled to room temperature.

The ion conducting (IC) solution was synthesized by adding an alcoholic solution of LiI (powder, 99.9%) + I_2 (99.8%, AR) to the hybrid ORMOSIL. The final solution was viscous with a yellow/brown color.[29,30]

Fabrication of the Asymmetric EC Devices. We prepared several EC devices with the configuration, ITO-coated-glass-1/h-WO_3/ICL/ITO-coated-glass-2, where the ITO (indium−tin oxide) coated glass slides are the two transparent electrodes used to apply the electric field, h-WO_3 is the EC layer, and ICL is the ion conducting and electronically insulating layer. On the ITO-coated-glass-1, a WO_3 film was deposited by dip-coating. The films were heated in air at 400 °C for 1 h. The ICL was applied on top of the WO_3 layers and the ITO-coated-glass-2 was pressed gently against this coating to ensure a uniform distribution of the ICL. After making the electrical connections, the EC device is ready for testing. The area of the EC devices was 5×2.5 cm^2.

Characterization. Transmission electron microscopy (TEM) of the WO_3 layers was preformed on a small amount of the film scrapped off the SiO_2-coated glass substrate and placed into a glass vial. Ethanol was added and the solution was sonicated for 10 min. A drop of the solution was placed onto a carbon-coated, 200 mesh copper grid and left to dry overnight. The sample was imaged using a 2011 JEOL STEM at 200 keV. Images were captured on a 4K × 4K multiscan CCD camera using Digital Micrograph from Gatan.

For scanning electron microscopy (SEM) characterization of WO_3 films and the EC devices, specimen cross sections were prepared and mounted vertically on 32 mm diameter aluminum specimen supports with conductive copper tape and colloidal graphite. Specimens were coated with ca. 150 nm of gold in a Hummer 6.2 sputtering unit (Anatech Ltd., Hayward, CA) and examined using a JEOL JSM-5600 SEM (JEOL USA, Peabody, MA). Images were collected using an accelerating voltage of 10 kV, at a working distance of 20 mm.

The crystal structure changes of the Li_xWO_3 layer in an operating electrochromic device as a function of the applied voltage ranging from 1.0 to 2.5 V were studied by micro-Raman spectroscopy. The h-WO_3 layer used in the fabrication of the EC device was also characterized. Raman spectra were recorded at room temperature with a Jobin-Yvon Labram HR microanalytical spectrometer equipped with a motorized *xy* stage and autofocus. The spectra were generated with 17 mW, 632.8 nm He−Ne laser excitation and dispersed with the 1800 grooves/mm grating across the 0.8 m length of the spectrograph. The laser power was 4 mW at the sample surface. The spectral resolution is estimated to be less than 0.5 cm^{-1} for a slit width of 150 μm and a confocal hole of 300 μm.

The crystal structure of the Li_xWO_3 layer in an operating EC device was determined by X-ray diffraction. These measurements were carried out in reflection with a custom-built $\theta-\theta$ diffractometer equipped with pyrolytic graphite monochromator and analyzer crystals. Cu Kα radiation with wavelength $\lambda = 0.154\,178$ nm was used for the measurements, and the data are shown as a function of the modulus of the scattering vector $q = 4\pi\lambda^{-1} \sin\theta$, where 2θ is the scattering angle. Air scattering was avoided by evacuating the sample space. Two samples were measured: an empty ITO-coated glass substrate and a substrate with a h-WO_3 layer coated on it. Subsequently, an EC device was assembled. The device was colored and bleached by applying voltages in the range from −2.0 to 2.5 V for 180 s. Prior to the next measurement, the top electrode was removed and the remaining ICL was wiped off with isopropyl alcohol. This sequence was repeated prior to all remaining measurements. The data were fitted to a series of the sum of

(26) Kuzmin, A.; Purans, J.; Cazznelli, E.; Vinegoni, C.; Mariotti, G. *J. Appl. Phys.* **1998**, *84*, 5515–5524.
(27) Pyper, O.; Kaschner, A.; Thomsen, C. *Sol. Energy Mater. Sol. Cells* **2002**, *71*, 511–522.
(28) Cazznelli, E.; Vinegoni, C.; Mariotto, G.; Kuzmin, A.; Purans, J. *J. Solid State Chem.* **1999**, *143*, 24–32.
(29) Kudo, T. *Nature* **1984**, *312*, 537–538.
(30) Stathatos, E.; Lianos, P.; Štangar, U. L.; Orel, B. *Adv. Mater.* **2002**, *14*, 354–357.

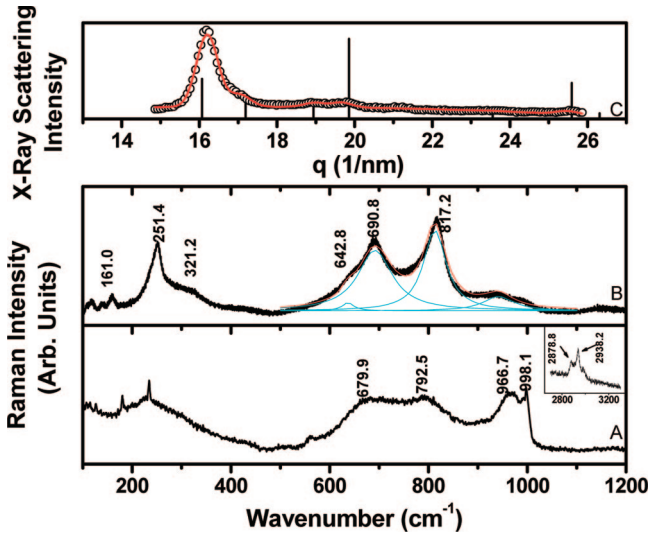

Figure 2. (A) Raman spectrum of the as-deposited WO_3 film, (B) the Raman spectrum of the h-WO_3 film obtained after heat treatment at 400 °C, and (C) the XRD pattern of the h-WO_3 film and the stick pattern of the h-WO_3 (JCPDS 33-1387). The solid line (Figure 2C) shows the fit to the XRD pattern.

Gaussian peaks, based on a hexagonal lattice, and a parabolic background. The peak width is determined by the fitted crystallite size and the measured resolution of the instrument. A fitted small offset in 2θ allows for small errors in sample and beam alignment.

Optical transmittance of the EC devices in their colored/bleached states was recorded at normal incidence with a Biochrom Ultrospec 2000 UV−visible spectrophotometer.

Results

Synthesis and Structural Characterization of the h-WO_3 Films. In this work, tungstic acid sols were prepared by mixing H_2O_2 and metallic tungsten powder. The ORMOSIL, used as a templating agent, was added to the tungstic acid sol, and the resulting sol was used for the WO_3 film coating. Figure 2A shows the Raman spectrum of the as-deposited WO_3 film on ITO-coated glass substrate. A broad band is observed with two humps at 679.9 and 792.5 cm^{-1}. Another broad band is seen at 966.7 cm^{-1} with a sharp feature at 998.1 cm^{-1}. These bands indicate that the as-deposited film is hydrated tungsten oxide.[31] The higher wavenumber (2700−3500 cm^{-1}) region of this spectrum shows the ν-CH_2 vibrational modes, emerging from the organic contents of ORMOSIL (see inset Figure 2A). ORMOSIL essentially consist of the product obtained by an acylation reaction between poly(propylene glycol)bis(2-aminopropyl ether) (2-APPG) with ICS. This template has facilitated the retention of the hydrated state of the as-deposited film. The as-deposited hydrated tungsten oxide films were annealed at 400 °C for 1 h. The Raman spectrum of the films after annealing at 400 °C is displayed in Figure 2B. The bands ascribed to lattice vibrations are observed below 200 cm^{-1}. The band observed at 251.4 cm^{-1} is assigned to δ(O−W−O) deformation vibrations, while the bands at 690.8 and 817.2 cm^{-1} are due to the ν(O−W−O) stretching vibrations. These bands are characteristic features of h-WO_3. The Raman peak positions of our h-WO_3 films are matching very well with those reported for h-WO_3 powder by Daniel et al.[32] The bands at 817.2 and 690.8 cm^{-1} appear broadened due to the nanocrystallite nature of the h-WO_3 films. The synthesis of the metastable h-WO_3 films is seriously limited by the very narrow range of annealing temperature and, hence, could only be obtained with nanocrystallite sizes. Even a small increase in the heat treatment at 450 °C results in the formation of a mixed h-WO_3−m-WO_3 phase, and a pure m-WO_3 phase is obtained at 500 °C.

The X-ray scattering of WO_3 layer, deposited on the ITO glass substrate and annealed at 400 °C for 1 h, is shown in Figure 2 C. The diffraction pattern corresponds to hexagonal WO_3, for which the JCPDS card 33-1387 is shown by the vertical bars.[33] We consider a doubled unit cell in the *c*-direction, and the corresponding indexing of the six marked peaks in Figure 2C is (002), (110), (102), (200), (112), and (202) from left to right. By fitting the diffraction patterns, we find the lattice constants *a* and *c* of the hexagonal phase to be 0.7379 ± 0.0008 and 0.7756 ± 0.0002 nm, respectively. Hexagonal WO_3 powder prepared by the procedures involving NH_4 has smaller lattice parameter ($c = 0.765$ nm)[18] than the value reported by Gerand et al. ($c = 0.7798$ nm).[17] However, in this work, the obtained lattice parameters are found to be closer to those reported by Gerand et al. The crystallite size is around 10 nm. The h-WO_3 film will be referred as "virgin h-WO_3" film for convenience.

SEM of the Virgin h-WO_3 Layer and the Cross Section of the EC Device. Figure 3A shows the cross-sectional image of the EC device. High surface area and pores in the WO_3 layer further the efficient operation of the EC device, through improved reaction kinetics. To fulfill the above-mentioned requirements a templating strategy based on ORMOSIL was used. During the heat treatment of the composite layer, the organic part of the template burns out, creating the pores in the film, while the SiO_2 acts as a skeleton, preventing the formation of cracks by binding the WO_3 particles together. In the SEM image, the macroporous structure of the virgin h-WO_3 layer, which is at the surface of the ITO-glass substrate, is evident (Figure 3A). The ITO layer is 190 ± 40 nm thick. The thickness of the virgin h-WO_3 layer used in the EC device was of 842 ± 50 nm, and a 12 ± 1 μm thick ICL is sandwiched between the h-WO_3 layer and a second ITO-coated glass slide.

TEM of the Virgin h-WO_3 Film. The morphology and microstructure of h-WO_3 layer coated on SiO_2-coated glass have been examined by TEM. Figure 3B shows the mesoporous structure of the walls separating the macropores in h-WO_3 film. The box in Figure 3B shows the lattice image, indicating the hexagonal features. Parts C and D of Figure 3 show the interplanar distances obtained by inverse FFT of lattice spacings from the region indicated by the box, which is found to be 0.72 and 0.79 nm, respectively. These lattice spacings correlate very well with those of h-WO_3.

(31) Nonaka, K.; Takase, A.; Miyakawa, K. *J. Mater. Sci. Lett.* **1993**, *12*, 274–277.

(32) Daniel, M. F.; Desbat, B.; Lassegues, J. C. *J. Solid State Chem.* **1987**, *67*, 235–247.

(33) Powder Diffraction Files Inorganic and Organic (Card No. 85-2460) (Hexagonal-WO_3). JCPDS-International Centre for Diffraction Data, PDF2 Data Base, Swarthmore, PA, 1996.

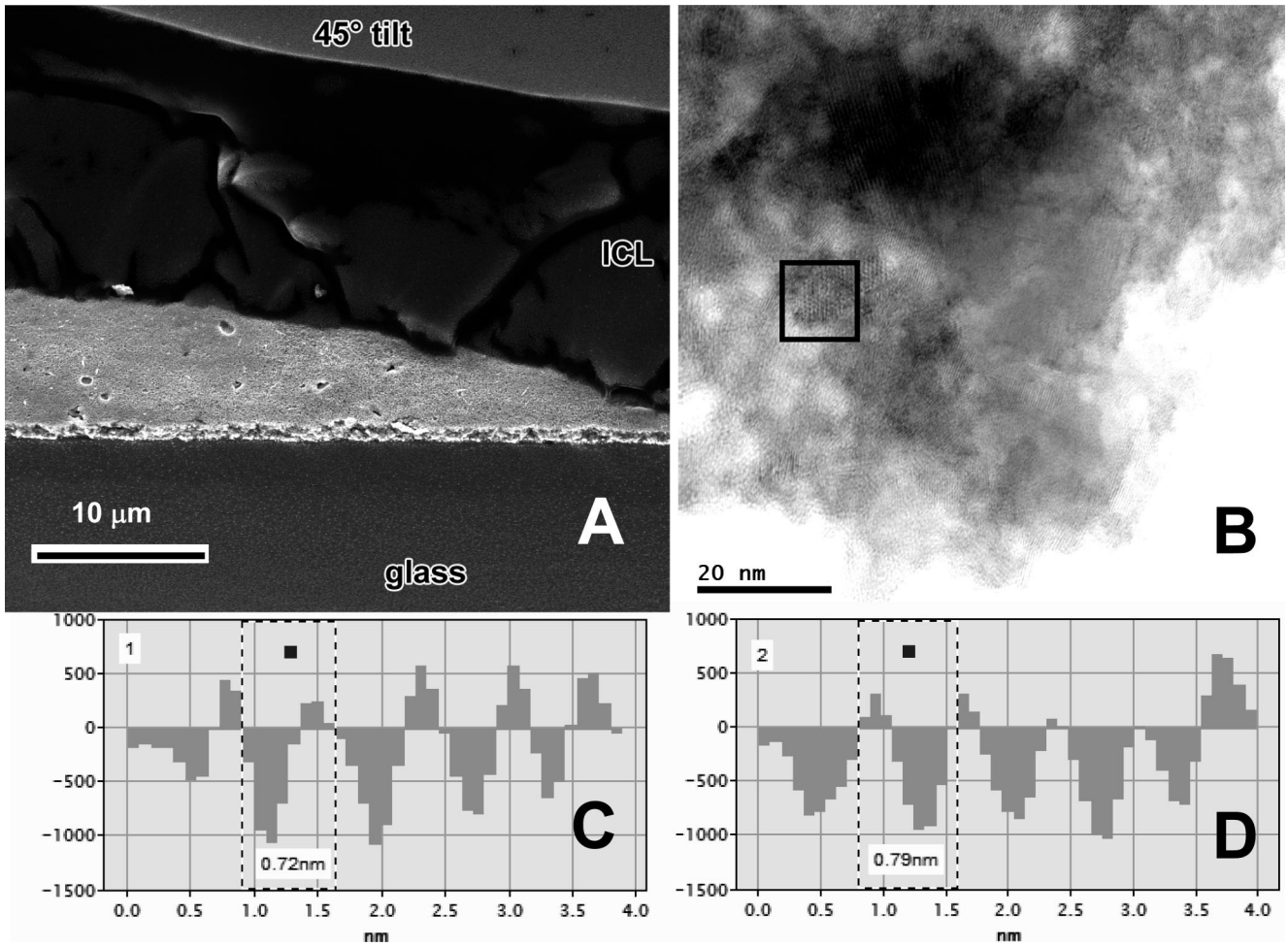

Figure 3. (A) SEM of the cross section of the device displaying the h-WO_3 layer on ITO-coated glass and the ion conducting layer and (B) TEM of the h-WO_3 layer with lattice spacings (C and D).

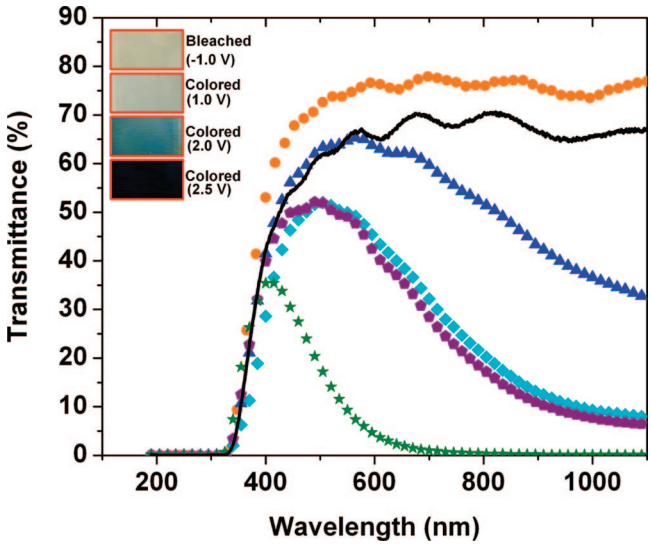

Figure 4. Optical transmittance of the EC device in the bleached state at −1.0 V (filled circles) and in colored states at applied potentials of 1.0 V (triangles), 1.5 V (diamonds), 2.0 V (pentagons), and 2.5 V (stars). The solid line shows the transmittance of the virgin h-WO_3. The inset in the figure shows actual digital photographs of the device in the bleached and colored states.

Optical Properties of the Electrochromic Device. Figure 4 shows the transmission spectra of an electrochromic device constructed by using h-WO_3 layer as an active working cathode in its colored and bleached states for applied potentials of ±1.0, ±1.5, ±2.0, and ±2.5 V. For comparison, the transmittance of the virgin h-WO_3 layer is presented as a solid line. The recorded transmission spectra of the device in the bleached state for potentials at −1.5, −2.0, and −2.5 V were indistinguishable from the spectrum of the device bleached at −1.0 V, clearly demonstrating the reversibility of the device. In the bleached state, the transmittance of the device at a wavelength 1100 nm was 76.9%. At coloration potentials of 1.0, 1.5, 2.0, and 2.5 V, the transmittance is reduced to 32.5, 7.9, 6.4, and 0.1%, respectively. The modulation of the transmittance of the device in the wavelength region above 800 nm is very important, as thermal energy radiated in the IR region falls into this range. The optical modulation of ∼76% above 800 nm obtained here is exceptionally high for EC devices.[3b] When the coloration potentials of 1.0, 1.5, 2.0, and 2.5 V are applied, the maximum transmittances are observed at 567, 502, 491, and 403.5 nm, respectively, and the transmittance fwhm are 709.5, 350.0, 341.0, and 147.0 nm, respectively.

It should be noted that the transmittance of the h-WO_3 layer is low by ∼10% when compared with the transmittance of the device in the bleached state. This reduction in the intensity is attributed to the volume scattering of light in the sample by the macroporous features. After the construction of the device, the ICL, which is smeared over the h-WO_3

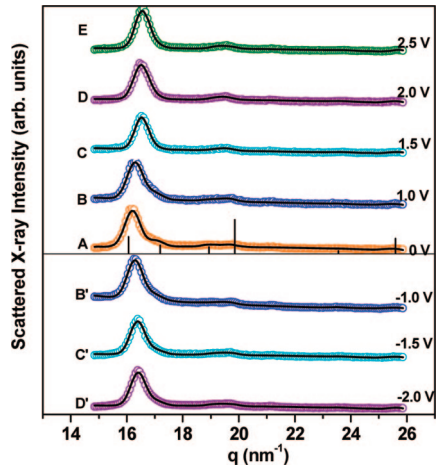

Figure 5. (A) XRD pattern of the macroporous h-WO_3 layer used in the fabrication of the EC device, and the XRD patterns of the device at coloration and bleaching potentials of ±1.0 V (B, B′), ±1.5 V (C, C′), ±2.0 V (D, D′), and 2.5 V (E). The solid lines show the fits to the XRD patterns.

layer, penetrates into its macropores and replaces the air voids. As ICL has higher refractive index than air (1.45 at λ = 589 nm), the medium is homogenized and it results in higher transmittance. The inset in Figure 4 shows actual digital photographs of the devices in the colored and bleached states. As the device transmits in the visible part of the spectrum and since we obtain strong controllable optical modulation in the region above 700 nm, this EC device based on macroporous h-WO_3 layer qualifies for applications in smart windows.

XRD Studies of the Operating Device. X-ray scattering patterns after intercalation and deintercalation of Li into the macroporous h-WO_3 layer of the EC device are shown in Figure 5. The diffraction pattern of the virgin h-WO_3 layer coated on the ITO-coated-glass-1 is shown in Figure 5A. Inserting and extracting lithium at different voltages shifts the diffraction peak positions. We determine the lattice constants *a* and *c* of the hexagonal phase for different sample states by fitting the diffraction patterns in Figure 5. Each spectrum is fitted to a series of Gaussian peaks superimposed on an overall quadratic background. These fits, shown as lines in Figure 5, closely match the experimental data points (open circles). The peak width Δq, assumed to be the same for all reflections, and the intensities of the individual peaks are treated as a fitting parameter. We correct the peak width for the instrument resolution and use it to estimate the crystallite size using the Scherrer method, assuming that, for example, crystallite-to-crystallite variations of the lattice parameter do not contribute to the peak widths. The fitted lattice parameters and crystallite sizes are shown in Figure 6 as a function of the voltage applied to the device prior to the measurement. We note that the lattice parameter *c* decreases during the sequence of measurements. The lattice parameter *a* remains initially the same, indicating that the unit cell volume decreases as the device ages during cycling. In the later part of the measurement cycle, with applied voltages of ±1.5 V and higher, we observe that the lattice constant *c* is significantly lower for the Li-intercalated state (positive voltages) and that *c* increases as the lithium ions are extracted. The crystallite size remains generally close to

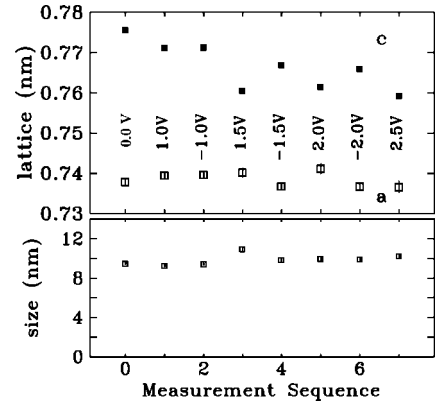

Figure 6. The changes in the lattice parameter and crystallites sizes of the h-Li_xWO_3 layer as a function of applied voltage from −2 to 2.5 V.

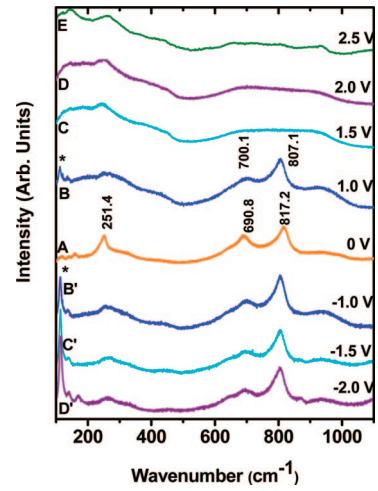

Figure 7. (A) Raman spectrum of the h-WO_3 layer used in the fabrication of the EC device, and Raman spectra of the device at coloration potentials of ±1.0 V (B, B′), ±1.5 V (C, C′), ±2.0 V (D, D′), and 2.5 V (E). * indicates the peaks originating from the ion conducting layer.

10 nm, with a possible slight increase during the measurement sequence. Following the ion insertion at 1.5 V we find a sharper peak in the data (Figure 5), which results in a larger apparent crystallite size. It is not clear what caused this effect. One possibility is a reduction of the slight variation of lattice parameters between different crystallites after intercalation.

Raman Studies of the Operating Device. Here we report the effects of the intercalation and deintercalation of Li into the h-WO_3 layer of an operating EC device as a function of applied voltages in the range from −2.0 to 2.5 V on the Raman spectra. Figure 7A, shows the Raman spectrum of the virgin h-WO_3 layer coated on the ITO-coated-glass-1. The bands located at 251.4 cm^{-1}, due to δ(O−W−O), and at 691.8 and 817.2 cm^{-1}, due to the ν(O−W−O), are the characteristic Raman modes of the h-WO_3.[32] By applying a potential of 1.0 V across the device, Li ions are intercalated from ICL into the h-WO_3 layer. Figure 7B shows the Raman spectrum of the EC device in its colored state after applying a voltage of 1.0 V. The mode at 690.8 cm^{-1} blue shifts to 700.1 cm^{-1}, whereas the mode at 817.2 cm^{-1} red shifts to 807.1 cm^{-1}. The intensity of the 251.4 cm^{-1} mode decreases significantly. Figure 7C−E shows the recorded Raman spectra of the EC device in the colored states (intercalating Li) at potentials of 1.5, 2.0, and 2.5 V, respectively. It can

be seen that, upon Li intercalation at these potentials, the modes due to the ν(O−W−O) stretching vibrations disappear. Correspondingly, by reversing the potential (−1.0, −1.5, and −2.0 V), the device reverts to its previous bleached state by deintercalating Li (Figure 3B′−D′). The recorded Raman spectra of the device in the bleached state were the same, clearly demonstrating the structural reversibility of the active layer of the EC device.

Discussion

Structural Changes Observed in the Raman Spectrum and in the XRD Pattern of the EC Device for the Applied Potential of 1.0 V. When Li ions are intercalated into the virgin h-WO_3 layer of the EC device at a potential of 1.0 V, XRD results show an increase in the lattice parameter *a* from 0.7379 to 0.7395 nm and a decrease in the lattice parameter *c* from 0.7756 to 0.7712 nm. Correspondingly, the recorded Raman spectrum of the EC device in the colored state at potential of 1.0 V shows a blue shift from 690.8 to 700.1 cm^{-1} and a red shift from 817.2 to 807.1 cm^{-1} of the bands related to O−W−O stretching. These blue and red shifts observed in the Raman spectrum, as well as the changes in the lattice parameters *a* and *c* obtained from XRD, indicate that the insertion of Li^+ into h-WO_3 induces a change in the bond length of O−W−O. Daniel et al. have obtained a correlation between frequency of vibration (force constant) and the bond length of W−O bonds. If tungsten is six-coordinated (W^{6+}) then the vibrational frequency increases with reduction in the bond length and vice versa. From our experimental data, it can be easily observed that the lattice parameter variations are reflected in the blue and red shifts of the O−W−O stretching modes.

As shown in Figure 1, in h-WO_3, Li^+ can occupy three possible sites, TC, HW, and SW. XRD measurements have been widely used to study the changes in the lattice parameter as a function of the amount of Li ions intercalated into h-WO_3. It has been reported that, for the ratio of Li/W = 0.4, the value of lattice parameter *c* reaches a minimum and remains constant up to the ratio of Li/W =1.0.[25] Figure 6 shows that, for the applied potential of 1.0 V, the lattice parameter *c* is 0.7712 nm and it reaches a minimum value of 0.7606 nm for the applied potential of 1.5 V. This indicates that, for a potential of 1.0 V across the EC device, the amount of Li^+ intercalates into the virgin h-WO_3 layer is <0.4, as the lattice parameter *c* has not reached the minimum value. Hibino et al. calculated electron energy levels in h-WO_3 and h-$LiWO_3$ by the DV-X α method and found the energies of Li ion insertion sites.[25] The results show that the site energy for TC is slightly less than that of HW and SW. Hence, the occupation of the TC is more probable and Li^+ insertion starts by filling TC sites. It should be noted that, according to Han et al.[24] and Hibino et al.,[25] direct intercalation of Li^+ into TC may not occur, as the distance between the three closely packed O atoms in the TC is too narrow, with a distance between O to the center of TC of 1.5 Å compared with the ionic radius of Li atom, 0.6 Å. Hence, for the applied potential of 1.0 V, Li ions enter into the TC through the hexagonal tunnel. In the process, in addition to the occupancy of the TC sites, some of the HW sites are also partially filled by Li ions.

Structural Changes Observed in the Raman Spectra and in the XRD Patterns for the Applied Working Potentials of 1.5, 2.0, and 2.5 V. Figure 7C−E shows the Raman spectra of the EC device in the colored states at the applied potentials of 1.5, 2.0, and 2.5 V. The spectra do not show any of the bands corresponding to the stretching ν(O−W−O) modes. When Li ions are intercalated into m-WO_3, the disappearance of O−W−O stretching bands in the Raman spectrum could be attributed to the formation of cubic Li_xWO_3.[6] The cubic phase can accommodate Li up to a maximum of $x = 0.76$. Even though the Raman spectra do not show any of the bands corresponding to the stretching ν(O−W−O) modes of the bridging oxygen, the XRD results show that the hexagonal framework of Li_xWO_3 is sustained for the coloration potentials of 1.5, 2.0, and 2.5 V (see Figure 5C−E). The stability of the hexagonal framework has been observed up to Li/W ratio of 1.45 during the electrochemical insertion of Li^+ into h-WO_3 powders.[10,23] As mentioned earlier, the lattice parameter *c* attains its minimum value when the Li/W ratio is 0.4 and remains unchanged up to a ratio of Li/W = 1.0.[25] Correspondingly, in our XRD studies *c* reaches a minimum value of 0.7606 nm when the applied potential is 1.5 V and remains unchanged as the potential is increased from 1.5 to 2.5 V. Thus, for the applied potentials of 1.5−2.5 V, the amount of Li that can be intercalated into the h-WO_3 layer of the EC device is between 0.4 and 1.0.

In order to understand the vanishing of the stretching ν(O−W−O) modes in the Raman spectra (Figure 7C−E) while the EC active layer still retains the hexagonal framework (h-Li_xWO_3), we consider the Li^+ occupancy in h-WO_3 for the applied potentials of 1.5, 2.0, and 2.5 V. For the applied potential of 1.0 V, trigonal cavity sites are filled, whereas the hexagonal windows are partially filled. By applying a potential of 1.5 V and above, the population of Li ions inside the hexagonal tunnel increases. In this scenario, Li ions inside the HW start moving toward the four-coordinated square window (SW) (see Figure 1B) in order to accommodate increased amount of Li ions. Hibino et al. have suggested that the location of Li ion near the SW is governed by the Li−Li ionic distances and the distance between the SW.[25] As there is no shielding for the Li ions, and Li−Li ionic distance is more than 5.5 Å, Li ions can only occupy alternate sites close to SW and it will lead to ordering of Li ions inside the h-WO_3. Hibino et al. have mentioned that for the Li/W ratios >0.4, the SW of the h-WO_3 start to be occupied, and in our case, this happens when the coloration voltages of 1.5 to 2.5 V are applied to the EC device.[25]

At this point, we want to draw attention to the transformation of h-WO_3 to m-WO_3. Figlarz has pointed out that needle crystals of h-WO_3 which lie on the [001] plane partially transformed to the monoclinic phase in a sample heat treated at 420 °C and quenched before the completion of the transformation.[10] This monoclinic phase was not observed inside the h-WO_3, but it was observed laterally. When the needle crystals of h-WO_3 were annealed at 420 °C for 5 h,

complete transformation to monoclinic was observed. This experiment has demonstrated that h-WO_3 and m-WO_3 have a definite plane that is common to both of phases, and an electron microscopy study showed that the plane is [100].[10] This topotactic nonpseudomorphous phase transition occurs from h-WO_3 to m-WO_3, because in the [100] plane the atomic arrangement is similar in both cases. In h-WO_3, the [100] plane, which contains the four-coordinated square window, resembles the [100] plane in m-WO_3. For the applied coloration voltages of 1.5, 2.0, and 2.5 V, which correspond to x values of 0.4−1.0, the Li ions move toward the SW. When the square windows are occupied by Li ions, the structure of h-Li_xWO_3 is isostructural with cubic Li_xWO_3 when visualized through the SW, which is lying in the [100] plane. Slade et al. have originally suggested that, in h-WO_3, as the concentration of Li is increased, the ions may move toward the SW in the [100] plane (Figure 1B).[23] This suggestion stems from the fact that there is enough room for the Li ion to move as the distance from the center of the hexagonal cavity to the square window is ∼3.2 Å, whereas the ionic radius of Li in a four-coordinate square window site is ∼0.5 Å. Further they suggested that the occupancy of Li ion into the four-coordinate square window is possible because the SW is isostructural to the four-coordinate sites occupied by Li in cubic $Li_{0.36}WO_3$. In m-WO_3, Li intercalation leads to cubic phase, and when the cubic phase is reached, O−W−O stretching modes vanish.[6] This occurs because, as Li ions are inserted into the m-WO_3, it transforms toward higher symmetric states such as tetragonal and cubic. Cubic Li_xWO_3, which is similar to ReO_3 structure, does not have Raman-active modes. It should be noted that the *ab* plane in WO_6 is already nearly symmetric. When Li is inserted into the square windows, the axial oxygen is also symmetrizised, which results in isostructural WO_6 octahedra, as seen in cubic-WO_3, and for this kind of structure Raman vibrations are forbidden.[34] Hence, when Li ions are intercalated into the h-Li_xWO_3 structure, for $x > 0.4$, Raman modes vanish and this intercalation was found to be reversible. XRD data, which shows a reduction in the lattice parameter c toward a as Li content is increased (Figure 6), also indicate that the symmetry is increasing in the local structure of WO_6 octahedron, within the hexagonal framework. Further, XRD shows that the hexagonal framework is retained even after the intercalation of Li up to 1.0, corresponding to the applied voltage of 2.5 V. Thus, Raman spectroscopic study in conjunction with XRD has clearly presented experimental evidence for the occupancy of Li ions into the four-coordinated square window sites of h-WO_3, as speculated by the earlier investigators.[23−25]

The Structural Changes of h-Li_xWO_3 Layer under Bleaching Conditions. According to the optical studies, the EC device exhibits excellent coloration/bleaching reversibility (see Figure 4). However, an interesting structural irreversibility is observed from the Raman and XRD studies. The Raman spectrum of the EC device in its colored state after applying a potential of 1.0 V shows ν(O−W−O) modes at 700.1 and 807.1 cm^{-1} (Figure 7B). These ν(O−W−O) modes disappear completely at coloration potentials of 1.5, 2.0, and 2.5 V (Figure 7C−E). By reversing the potential (−1.0, −1.5, − 2.0, and −2.5 V), the device reverts to bleached state by deintercalating Li (Figure 7B′−D′). But the Raman spectra of the device in the bleached state are identical to the Raman spectrum of the device colored at a potential of 1.0 V. This indicates that the spectrum in the bleached state is not identical to that of the virgin h-WO_3. In contrast to the EC device based on the m-WO_3 layer, where a complete deintercalation has been observed, the EC device based on the h-WO_3 layer does not exhibit the same full reversibility. Han et al.[24] and Hibino et al.[25] have reported that a complete deintercalation is impossible from the h-WO_3 under moderate deintercalation potentials of −1.0 to −2.5 V. This can be explained from the fact that the Li ion intercalating into a trigonal cavity is bound too tightly for deintercalation. During the bleaching cycle, the energy required for the extraction of Li from a trigonal cavity is higher than the energy required to intercalate into a TC of h-WO_3. This is supported by XRD, which shows that the lattice parameters c does not revert to its original value after intercalation at 1.5 V. The reversible characteristic of the EC device based on the structural changes evidenced from Raman and XRD data indicates that the EC coloration is mainly due to the occupancy of Li ions in HW as well as in four-coordinated square windows.

Conclusions

A WO_3 coating sol was prepared from tungstic acid sol in the presence of ORMOSIL as a templating agent. WO_3 films were dip-coated on ITO-coated glass substrates, and upon annealing at 400 °C, for 1 h, macroporous, crack free h-WO_3 films of up to ∼850 nm thickness, with crystallite size of ∼10 nm and lattice parameters of $a = 0.7379 \pm 0.0008$ nm and $c = 0.7756 \pm 0.0002$ nm, were obtained. Thus prepared h-WO_3 film on ITO-coated glass substrate was used as an active EC layer in the construction of an asymmetric EC device. Coloration and bleaching of the EC device was achieved by intercalating and deintercalating Li into the h-WO_3 EC layer at applied potentials of ±1, ±1.5, ±2.0, and ±2.5 V. Detailed XRD and micro-Raman studies were performed during Li intercalation and deintercalation. XRD measurements show systematic changes in the lattice parameters as a function of the applied potential and, at the same time, retention of the hexagonal framework. The changes in the lattice parameters is associated with the amount of Li intercalated into the h-WO_3 layer of the device, and this amount was found to be <0.4 for an applied potential of 1.0 V and $0.4 \leq x \leq 1.0$ for the applied potentials ranging from 1.5 to 2.5 V. Correspondingly, upon intercalation at potential of 1.0 V, the Raman spectrum shows red and blue shifts of the stretching O−W−O bands when compared with the virgin h-WO_3 layer. At this potential, Li ions completely fill TC and partially fill HW sites. As the coloration potential is increased to 1.5, 2.0, and 2.5 V, the bands corresponding to ν(O−W−O) modes completely vanish. The vanishing of the Raman modes shows that Li ions are inserted into the hexagonal cavity as well as into

(34) Stachiotti, M. G.; Corà, F.; Catlow, C. R. A.; Rodriguez, C. O. *Phys. Rev.* **1997**, *B55*, 7508–7514.

the four-coordinated SW, resulting in the formation an isostructural WO_6 octahedra, as seen in cubic-WO_3, and for this kind of structure, the Raman vibrations are forbidden.

When the Li ions are deintercalated under reversible voltages, the recorded Raman spectra of the device in the bleached state were identical to the Raman spectrum of the device colored at a potential of 1.0 V. This shows that, during the deintercalation, initial h-WO_3 phase is not recovered as the Li ions from the TC are not completely removed. However, optical measurements showed that the device is fully bleached. This leads to the conclusion that the coloration of the EC device is mainly due to the Li ions that occupy HW sites and four-coordinated square windows sites in h-Li_xWO_3 structure. Optical transmittance studies performed on the EC device as a function of applied potentials of ± 1, ± 1.5, ± 2.0, and ± 2.5 V, show excellent contrasts between colored and bleached states (e.g.76% for 2.5 V) and qualify the device for EC smart window applications.

Acknowledgment. The financial support of the Research Assistantships Initiative of New Brunswick Innovation Fund (NBIF), the Atlantic Innovation Fund (AIF-Round II), and National Science and Engineering Research Council (NSERC) of Canada is gratefully acknowledged. We thank Mr. James Ehrman (Digital Microscopy Facility, Mount Allison University, Sackville, NB, Canada) for the SEM measurements and Dr. Louise Weaver (Microscopy Microanalysis Facility, University of New Brunswick, Fredericton, NB, Canada) for the TEM measurements. We are thankful to Prof. Jacques Robichaud, Université de Moncton—Campus de Shippagan, Moncton, Canada, for his suggestions during the preparation of the manuscript.

CM8034455